XMM-Newton CCF Release Note

XMM-CCF-REL-168

EPIC absolute astrometry

B. Altieri

May 21, 2004

1 CCF components

Name of CCF	VALDATE (start of val. period)	EVALDATE (end of val. period)	List of Blocks changed	CAL VERSION	XSCS flag
XMM_BORESIGHT_0018	2000-01-01 00:00:00		BORESIGHT		NO

2 Analysis

To support the new vignetting correction implemented in SAS6, the optical axis for each camera had to be moved (in the MISCDATA CCF) and as a consequence new BORESIGHT Euler angles had to be regenerated from scratch in BORESIGHT issue 17. The determination of the new Euler angles was based on one single field : OMC2/3, in revolution 598, a rich stellar field, using the task `epicbscalgen` trying to reproduce the SAS 5.4 astrometry as far as possible. See XMM-CCF-REL-156, for more details.

A more global study was then necessary to investigate any systematic residual errors in these new Euler angles, translating into systematic shifts of the absolute astrometry in camera coordinate system (or in spacecraft coordinate system).

A bulk reprocessing of 430 ODFs was performed with SAS6 and the new BORESIGHT issue 17. Observations after revolution 500 were selected, where the attitude reconstruction algorithms from Flight Dynamics have been tuned to the best since launch.

Source detection was done with `edetect_chain` with a maximum likelihood threshold of 15. For each observation the absolute shift from the XMM frame to the optical is assessed by cross-correlating the source lists for each camera with the 2MASS NIR catalogue, which astrometric accuracy is estimated to be better than 0.2 arcsec.

A cross-correlation radius of 5 arcsec was used, associating the nearest NIR source as the most

Instrument	Y-axis rotation (arcsec)	Z-axis rotation (arcsec)	PHI angle delta (radian)	Theta angle delta (radian)
MOS1	1.1	0.42	-2.036 10^{-6}	5.333 10^{-6}
MOS2	0.72	0.17	-8.431 10^{-7}	3.490 10^{-6}
pn	0.35	0.0	0	1.696 10^{-6}

Table 1: Delta to previous BORESIGHT rotation around axis (arcsec) and delta to Euler angles (radians).

probable counterpart of the X-ray source. A frame offset was determined when two or more sources with optical counterpart were found, this was the case for about 210 observations. The offset is then projected into the camera coordinate system, with a simple rotation of the position angle.

The source densities in X-ray and in NIR are highly variable depending on the type of field (galactic/extragalactic) and the depth of the exposure in X-ray. But with typical source densities of 0.05 source/square arcmin (MOS1) and 1 source/square arcmin in 2MASS, there is a 2% probability of chance correlation with a NIR source in a radius of 5 arcsec. Hence the probability to have two random correlations is < 0.1

A special care was taken to remove all galaxy cluster and Supernovae Remnants observations, as they tend to return high densities of completely fake sources and therefore small and wrong offsets, with this processing (as well as CALCLOSED exposures !).

The offset scatter plots and corresponding histograms of the distributions are presented in figures 1 and 2. Some systematic offsets principally along the spacecraft Z-axis are evidenced.

3 Changes

The systematic offset found were corrected and implemented as delta variations in the Euler angles in BORESIGHT issue 18, using the SAS task `newsiam`.

The shifts in arcsec around the +Y and +Z axis and derived delta in Euler rotation angles are given in table 1.

4 Scientific Impact of this Update

A new bulk reprocessing with 1095 ODFs, from revolution 500 up to 767, was performed. An offset of the camera frame could be determined for about 850 observations, and for 600 observations with two or more optical counterparts. It can be verified in figures 3 & 4, (equivalent of figures 1 & 2 but with BORESIGHT CCF issue 18 this time), that no systematic offsets are left with this new CCF. The mean shift from the EPIC frames to the optical reference in on average null, in spacecraft coordinate system.

The same type of offset plots in Right Ascension/Declination axis would always show a mean

shift around zero, whatever systematics left in BORESIGHT Euler angle due to the position angle averaging.

Finally the same study was performed with the old SAS 5.4 and previous related BORESIGHT CCF issue 16, used until SAS6 was live. The same scatter plots and histograms of distributions are shown in figures 5 & 6. Some small (< 0.6 arcsec) systematic offsets were present,but different from (SAS6/BORESIGHT 17).

Note that with SAS5.4/BORESIGHT 16, the standard deviation of the offsets per axis was closer to 1.0 arcsec, compared to 1.2 arcsec with SAS6/BORESIGHT 18. This points probably to a Position Angle error, i.e. an slight error in the BORESIGHT PSI Euler in issue 18.

Note that the scatter on the spacecraft Z-axis (facing the sun) is significantly higher (wider gaussian) than on the Y-axis. This seems to be due a surprising seasonal dependence of the shifts, along the Z-axis: +0.7 arcsec in the revolution range 500-600, but -0.7 arcsec in the revolution range 600-700, as can be appreciated on figure 7 & 8. There is no explanation to this effect yet.

5 Estimated Scientific Quality

With this new BORESIGHT CCF the absolute astrometry is slightly changed at the arcsec level. It is now optimized such that on average the mean shift to the optical frame is close to zero, as demonstrated in figure 4.

A direct X-ray source position correlation between bright sources with a total number of counts higher than 500 in the central area (MOS central CCD) in all observation processed was performed. Such sources have coordinates errors due to the statistical uncertainty of the measurement lower than 0.5 arcsec for MOSs and lower than 0.7 arcsec for EPIC-pn (see figure 9). Hence they provide a better handle on systematics characterisation. The distribution of position offsets for these bright sources in the between EPICs is shown in figure 10.
The standard deviation is ∼0.6 arcsec per axis, hence a median offset between the two cameras for bright sources lower than 1.0 arcsec.

However some systematic shifts are evidenced between cameras along the spacecraft Y-axis in figure 10: 0.3 arcsec between MOS1 and pn, 0.2 arcsec between MOS1 and pn, and 0.5 arcsec between MOS2 and EPIC-pn which were not seen previously in figure 4 (null shift on average with the optical). The same type of systematic shift between cameras is seen when selecting sources over the whole field-of-view, instead of the central area. The origin of these camera-camera shifts is unexplained and somewhat inconsistent with the absolute astrometry analysis above.

Figure 4 shows a distribution width of offsets of 1.2 arcsec per axis. However this distribution includes on top of a systematic distribution a statistical component due to the fact that relatively faint X-ray sources have been used for the cross-correlation. With a typical number of sources of 5 per field the error on each camera offset per observation is of the order or 0.7-1.0 arcsec, hence widening the gaussian distribution.

By selecting subset of observations with a minimal threshold of 10 optical counterparts, the statistical error of each offset goes down to 0.4 arcsec on average, for an average number of optical counterparts of 20-25. The histogram of distribution of offsets per axis for this representative

subset of observations is presented in figure 11. Although the statistics is obviously much lower, the standard deviations of the gaussian distribution now go down to 0.7-0.8 arcsec per axis for the MOSs and even 0.6 arcsec for EPIC-pn, i.e. similar to figure 10.

Therefore 0.6 arcsec per axis is most probably the best estimate of the systematic component of the absolute astrometric accuracy of XMM-Newton. Hence this analysis indicates that **the XMM-Newton absolute astrometric accuracy is better than 1.0 arcsec** (or similarly a **FWHM of $\sim$ 2 arcsec**.), as can be seen in figure 12 in the case of EPIC-pn.

This statemement is true for observations acquired after revolution 500, and probably for earlier observations too, once repreocessed with the latest attitude software from Flight Dynamics. Note that this is significantly better than the early results of Tedds & Watson (2001), based on observations at the beginning of the mission.

6 Test procedures & results

See previous sections. SAS6.0 and SAS5.4 were used to compare the different performances of the BORESIGHT CCF issues 16, 17 & 18.

7 Expected Updates

No attempt has been made in this study to search for residuals in position angle rotations (i.e. Euler Psi angle), while some eraly evidences have been shown (J. Tedds) that with BORESIGHT issue 17 and hence also with new issue 18, a residual of 0.1 degree would be present. The slightly largest standard deviation fond with SAS6/BORESIGHT 18 vs SAS5.4/BORESIGHT 16 also points in that direction.

An error of 0.1 degree in the Euler PSI angle would lead to shifts up to 1.5 arcsec at the edge of the XMM field-of-view. It is not clear at this stage if this rotation error would apply to a particular camera, as it was the case for EPIC-pn in the past or to all cameras. This should be the subject of a subsequent analysis using the SAS task `eposcorr`.

8 References

"Improved Vignetting Correction by refining the XMM optical axis", M. Kirsch, XMM-CCF-REL-156, January 27, 2004,

"Absolute astrometry of XMM-Newton fields: *eposcorr* results", J. Tedds & M. Watson, SSC-LUX-TN-0060, issue 1.0, 13/11/2001

"EPIC MOS metrology", B. Altieri, XMM-CCF-REL-168, issue 1.1, 14 May 2004.

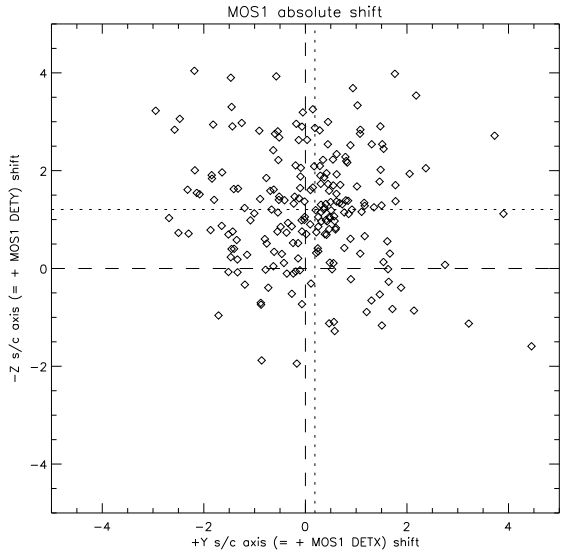

N obs = 211
DETX median = 0.18 RMS = 1.21
DETY median = 1.20 RMS = 1.18

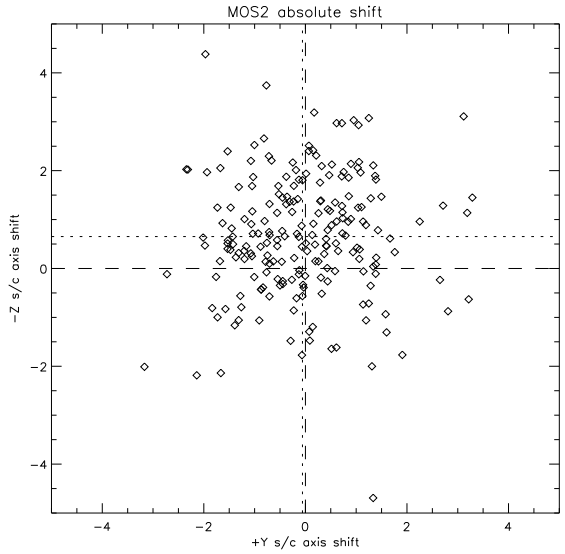

N obs = 210
DETX median = −0.0 RMS = 1.16
DETY median = 0.65 RMS = 1.24

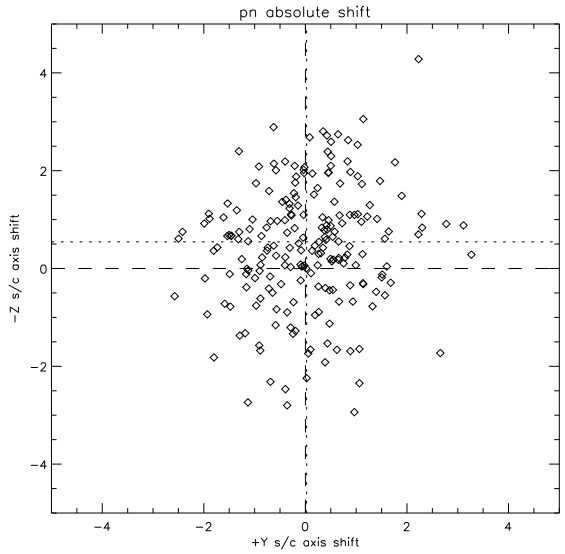

N obs = 207
DETX median = 0.02 RMS = 1.06
DETY median = 0.54 RMS = 1.24

Figure 1: Scatter plot of the offsets of the EPIC frame with the 2MASS reference frame for each EPIC camera projected in spacecraft coordinate system, one point per observation, with **BORESIGHT CCF v17**; Top panel: MOS1, Middle: MOS2, Bottom: EPIC-pn.

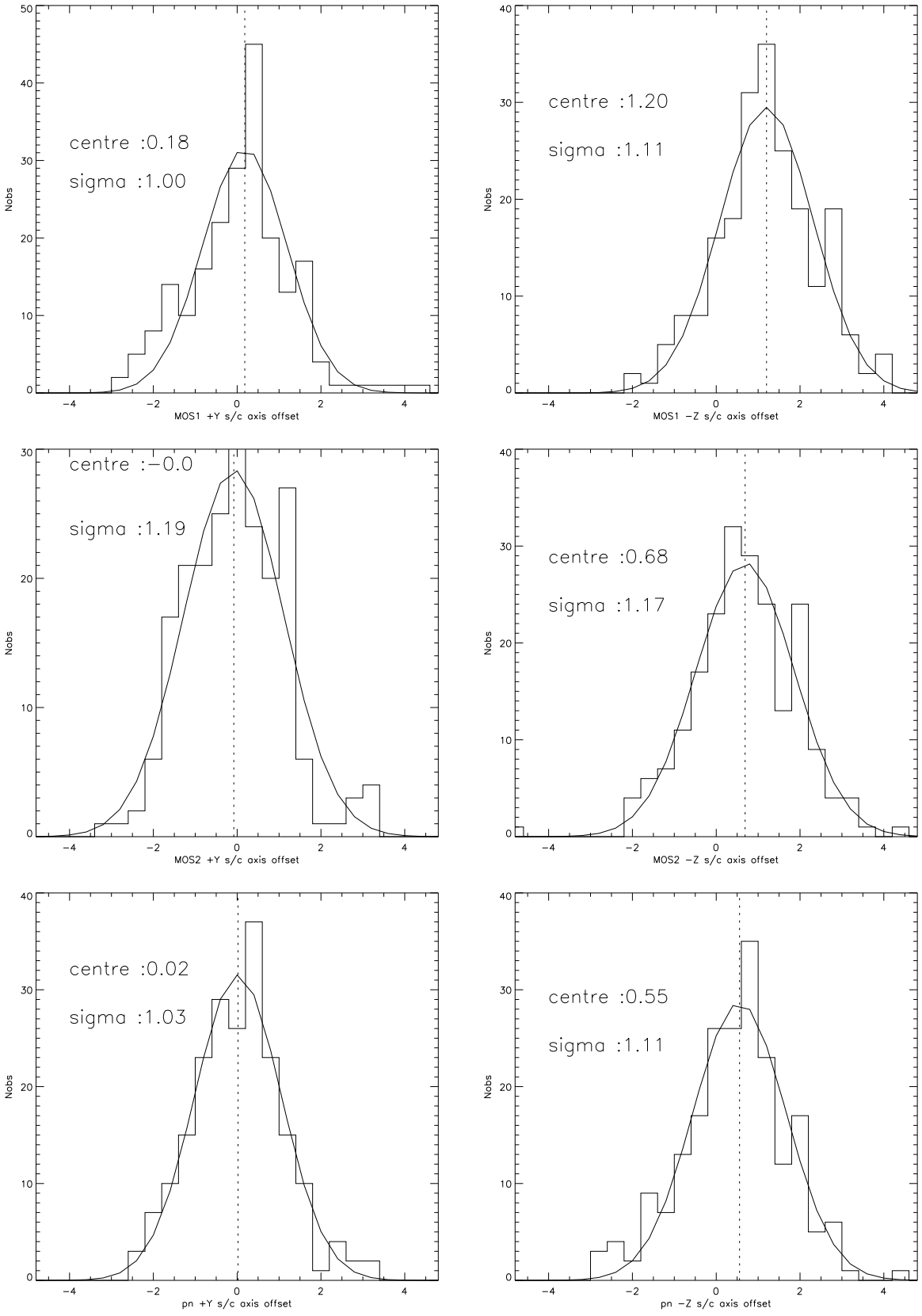

Figure 2: Histogram of the distribution of the offsets with the 2MASS reference frame for each EPIC on the two spacecraft axis with **BORESIGHT CCF v17**; Top panel: MOS1, Middle: MOS2, Bottom: EPIC-pn.

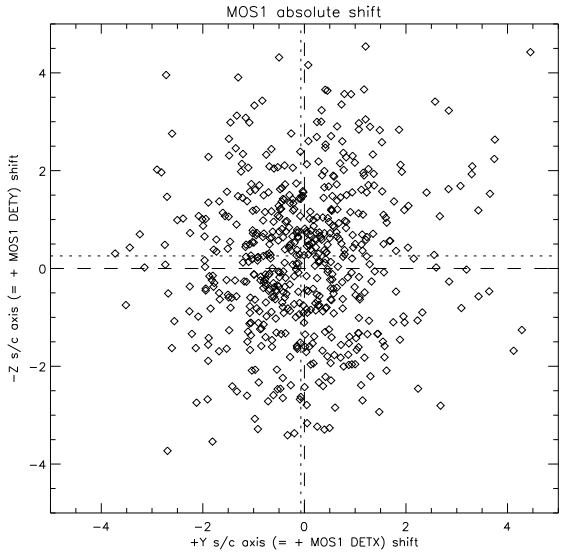

N obs = 572
DETX median = −0.0 RMS = 1.25
DETY median = 0.25 RMS = 1.52

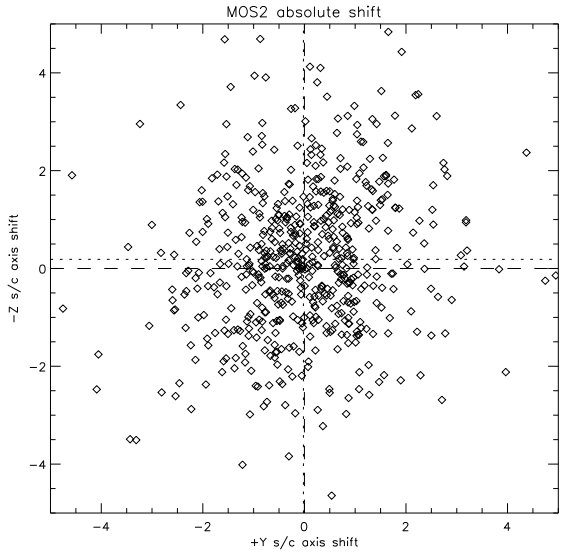

N obs = 584
DETX median = −0.0 RMS = 1.32
DETY median = 0.18 RMS = 1.51

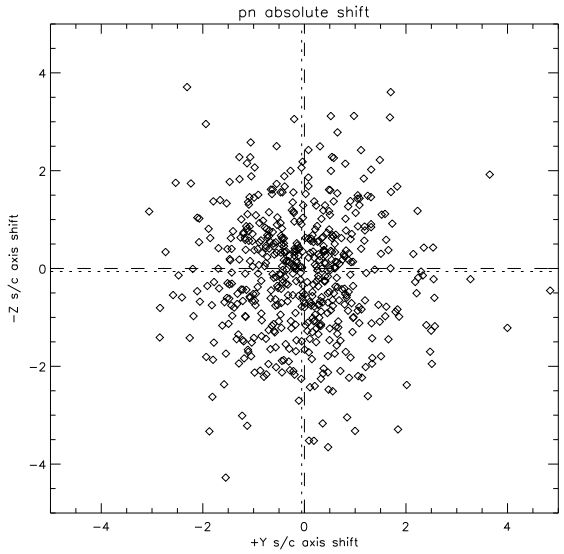

N obs = 547
DETX median = −0.0 RMS = 1.08
DETY median = −0.0 RMS = 1.25

Figure 3: Scatter plot of the offsets of the EPIC frame with the 2MASS reference frame for each EPIC camera projected in spacecraft coordinate system, one point per observation, with **BORESIGHT v18**; Top panel: MOS1, Middle: MOS2, Bottom: EPIC-pn.

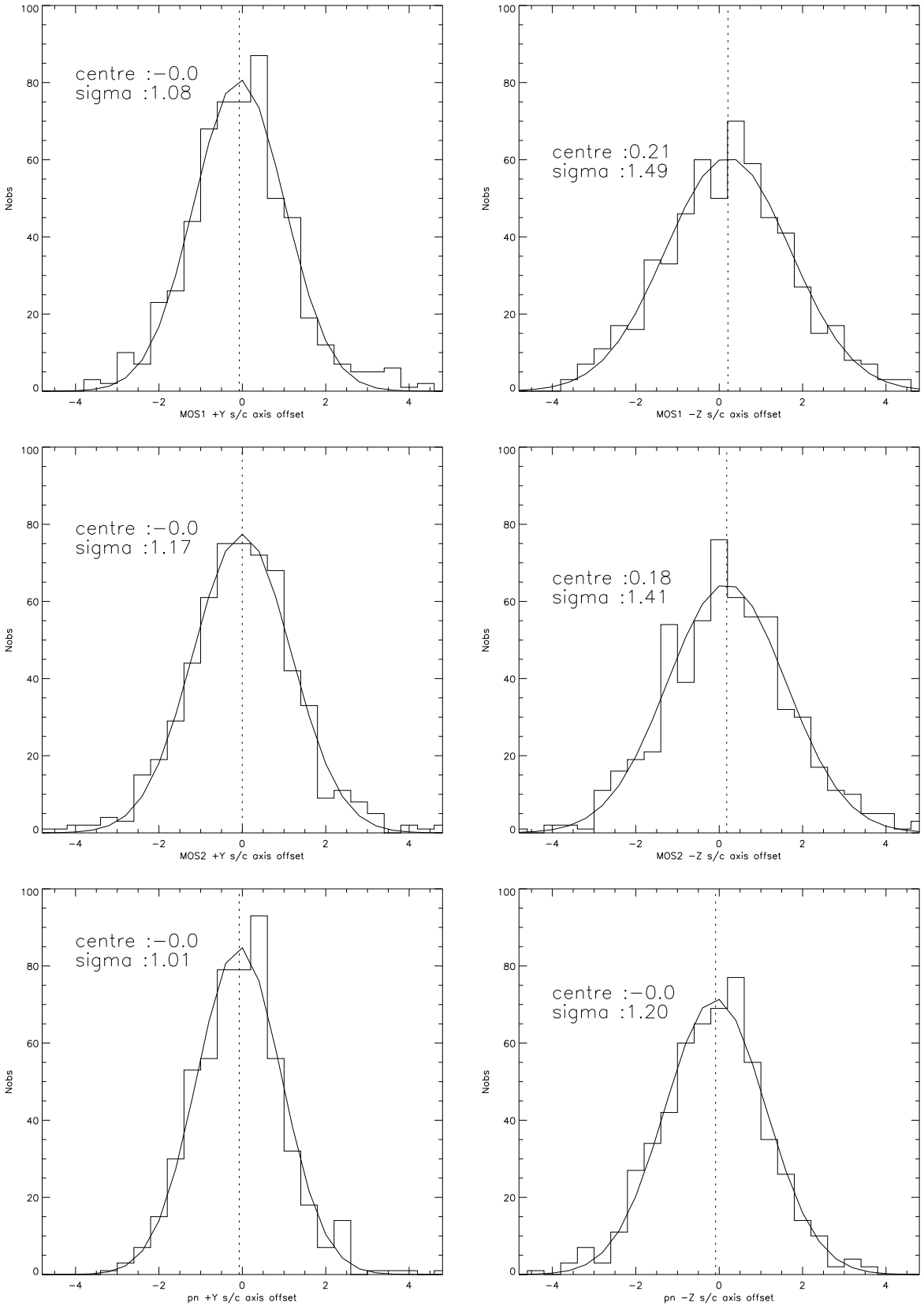

Figure 4: Histogram of the distribution of the offsets with the 2MASS reference frame for each EPIC on the two spacecraft axis with **BORESIGHT CCF v18**; Top panel: MOS1, Middle: MOS2, Bottom: EPIC-pn.

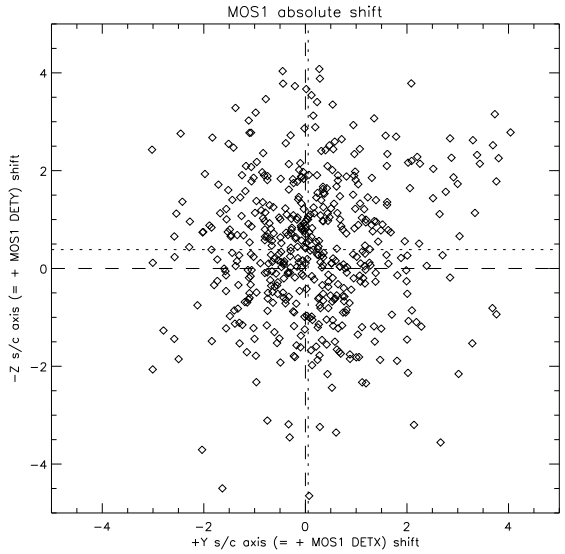

N obs = 496
DETX median = 0.05 RMS = 1.24
DETY median = 0.38 RMS = 1.42

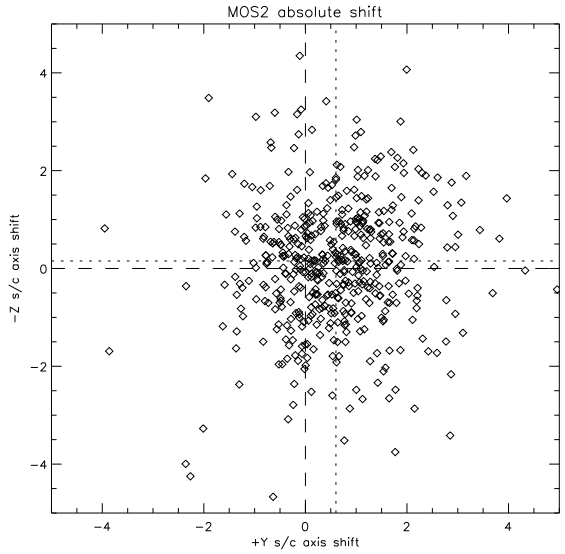

N obs = 488
DETX median = 0.60 RMS = 1.12
DETY median = 0.15 RMS = 1.29

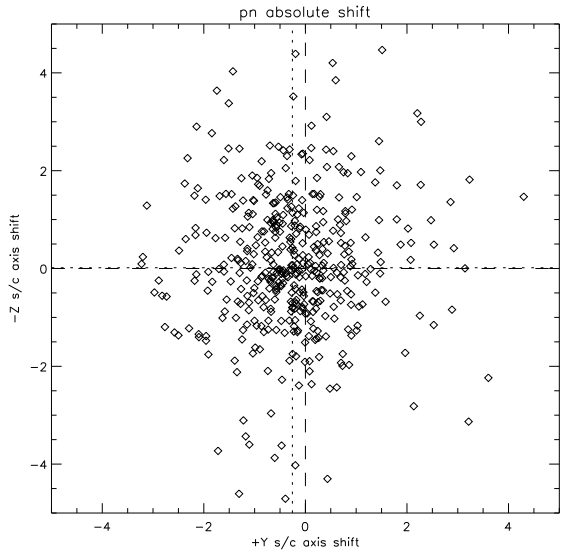

N obs = 432
DETX median = −0.2 RMS = 1.12
DETY median = 0.01 RMS = 1.41

Figure 5: Scatter plot of the offsets of the EPIC frame with the 2MASS reference frame for each EPIC camera projected in spacecraft coordinate system, one point per observation, with SAS 5.4 and **BORESIGHT CCF v16**; Top panel: MOS1, Middle: MOS2, Bottom: EPIC-pn.

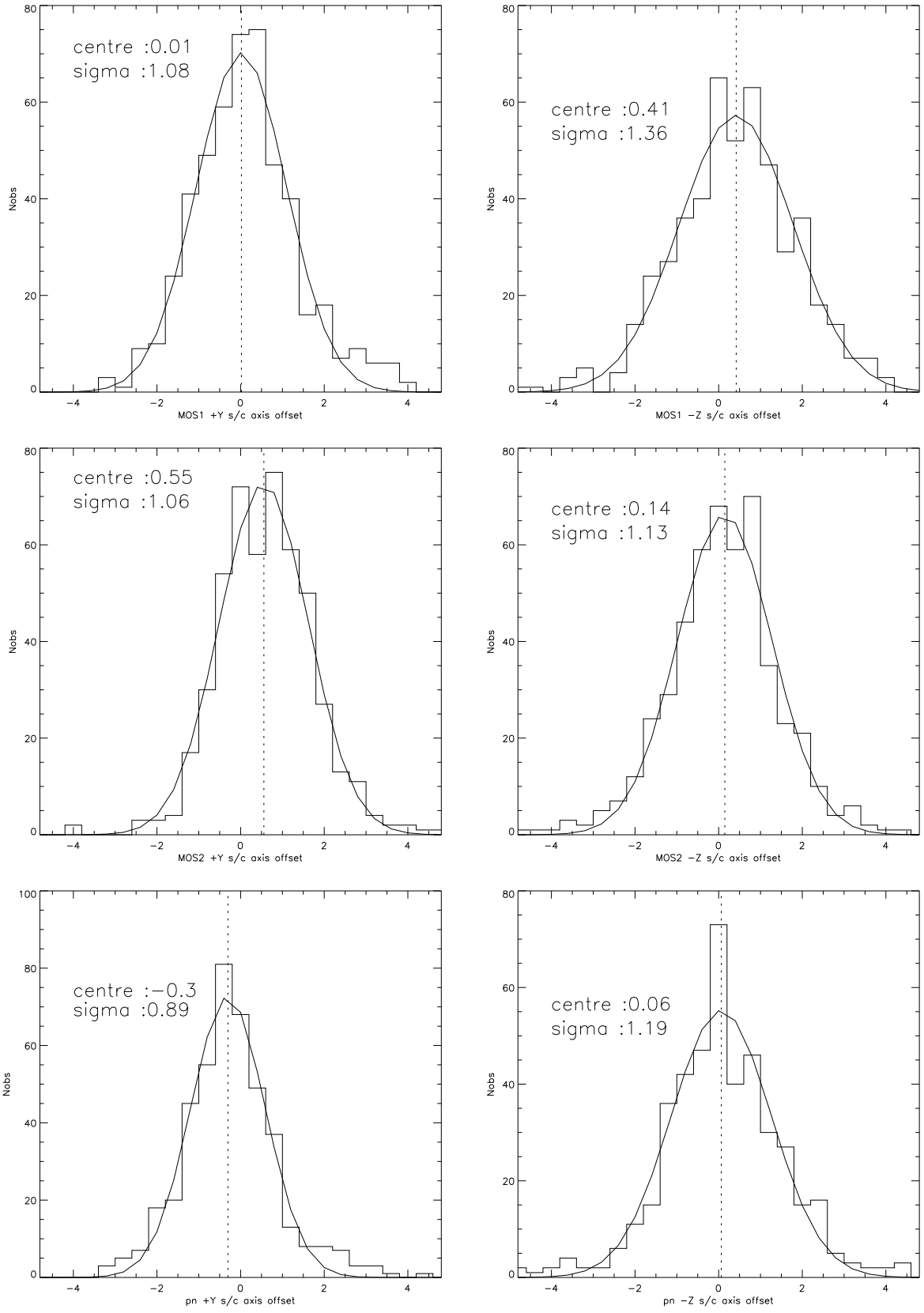

Figure 6: Histogram of the distribution of the offsets with the 2MASS reference frame for each EPIC on the two spacecraft axis with SAS 5.4 and **BORESIGHT CCF v16**; Top panel: MOS1, Middle: MOS2, Bottom: EPIC-pn.

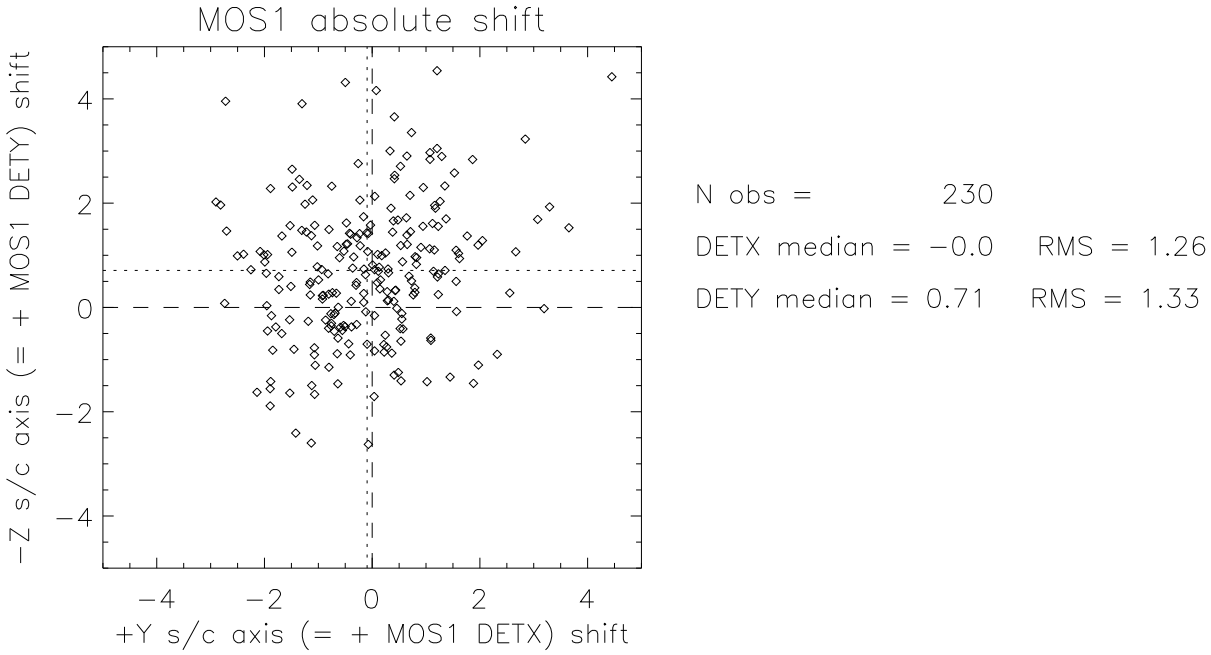

Figure 7: Scatter plot of the offsets of the EPIC frame with the 2MASS reference frame for MOS1 projected in spacecraft coordinate system, one point per observation, with BORESIGHT v18 in the **revolution range 500-600**

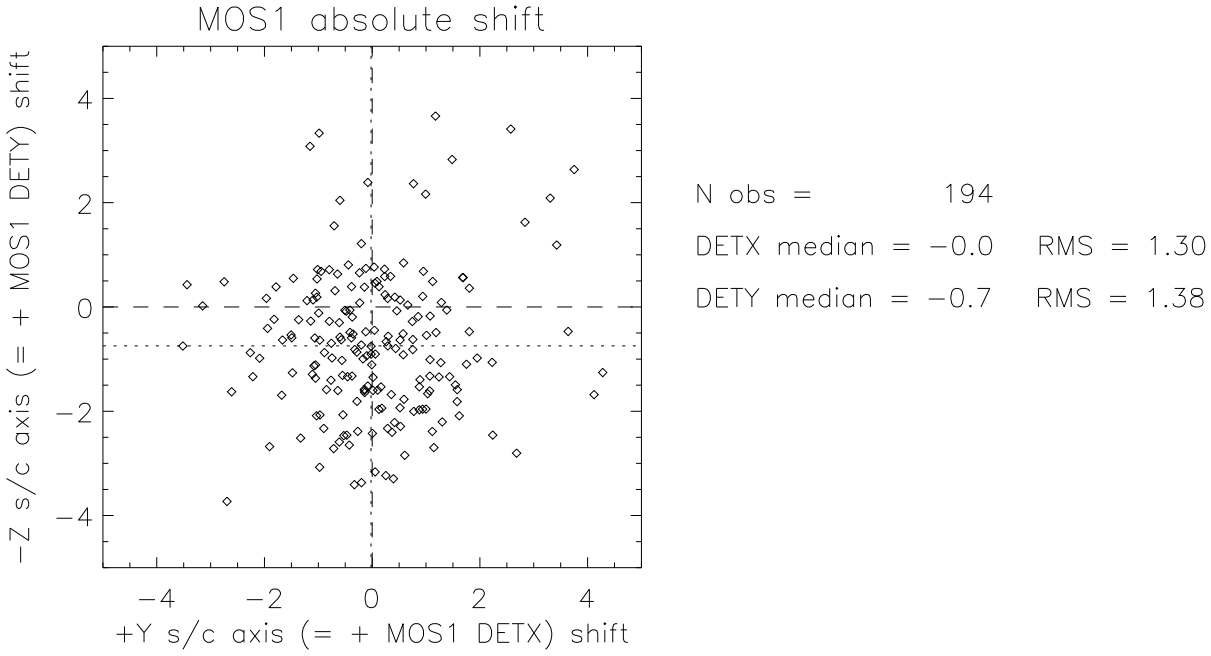

Figure 8: Scatter plot of the offsets of the EPIC frame with the 2MASS reference frame for MOS1 projected in spacecraft coordinate system, one point per observation, with BORESIGHT v18 in the **revolution range 600-700**

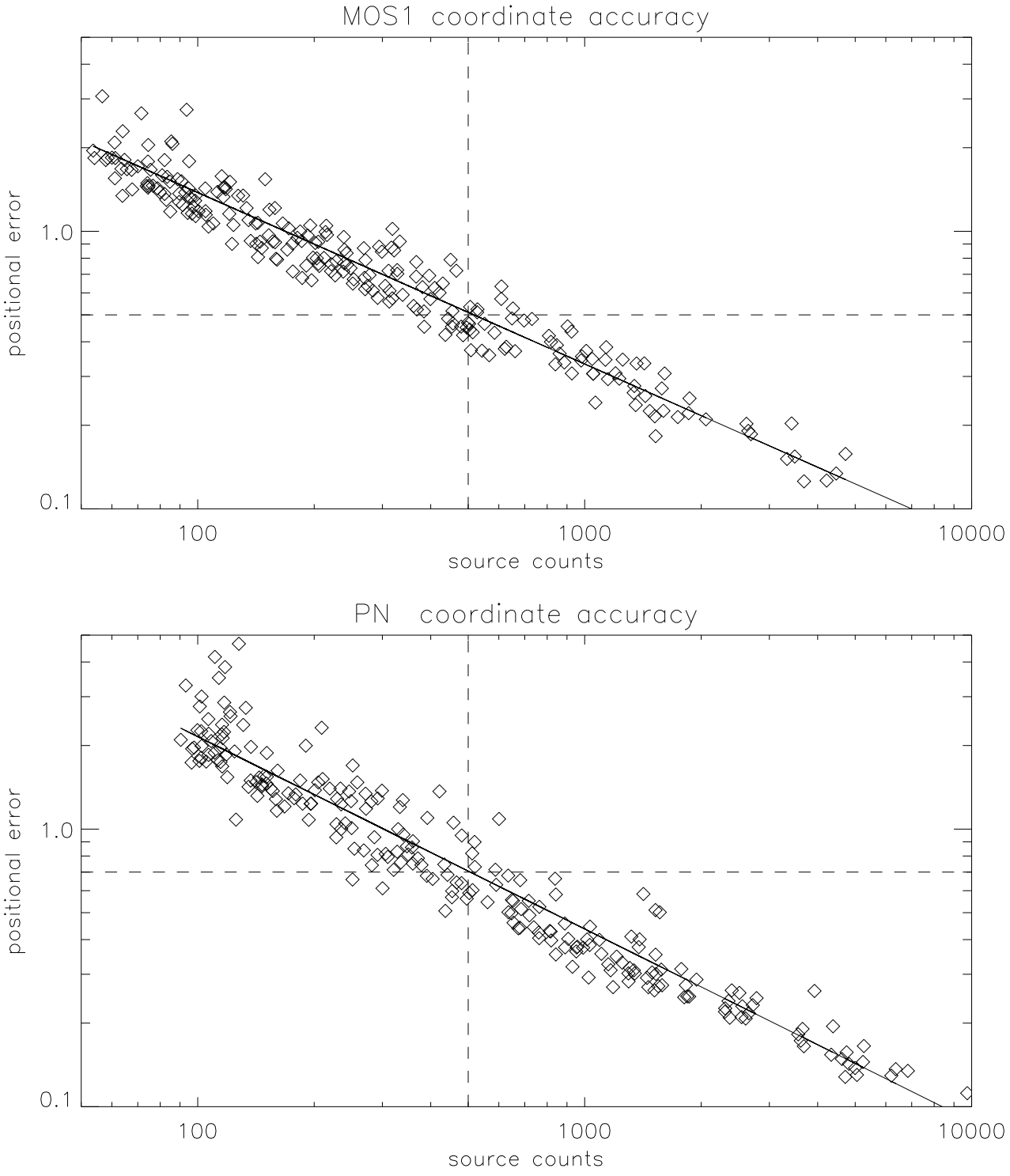

Figure 9: Coordinate errors returned by the SAS (`emldetct`) for sources as a function of source counts. The limitation is purely due to the statistical accuracy of the measurement. It is better for MOSs because of the smaller pixel size (1.1" vs 4")

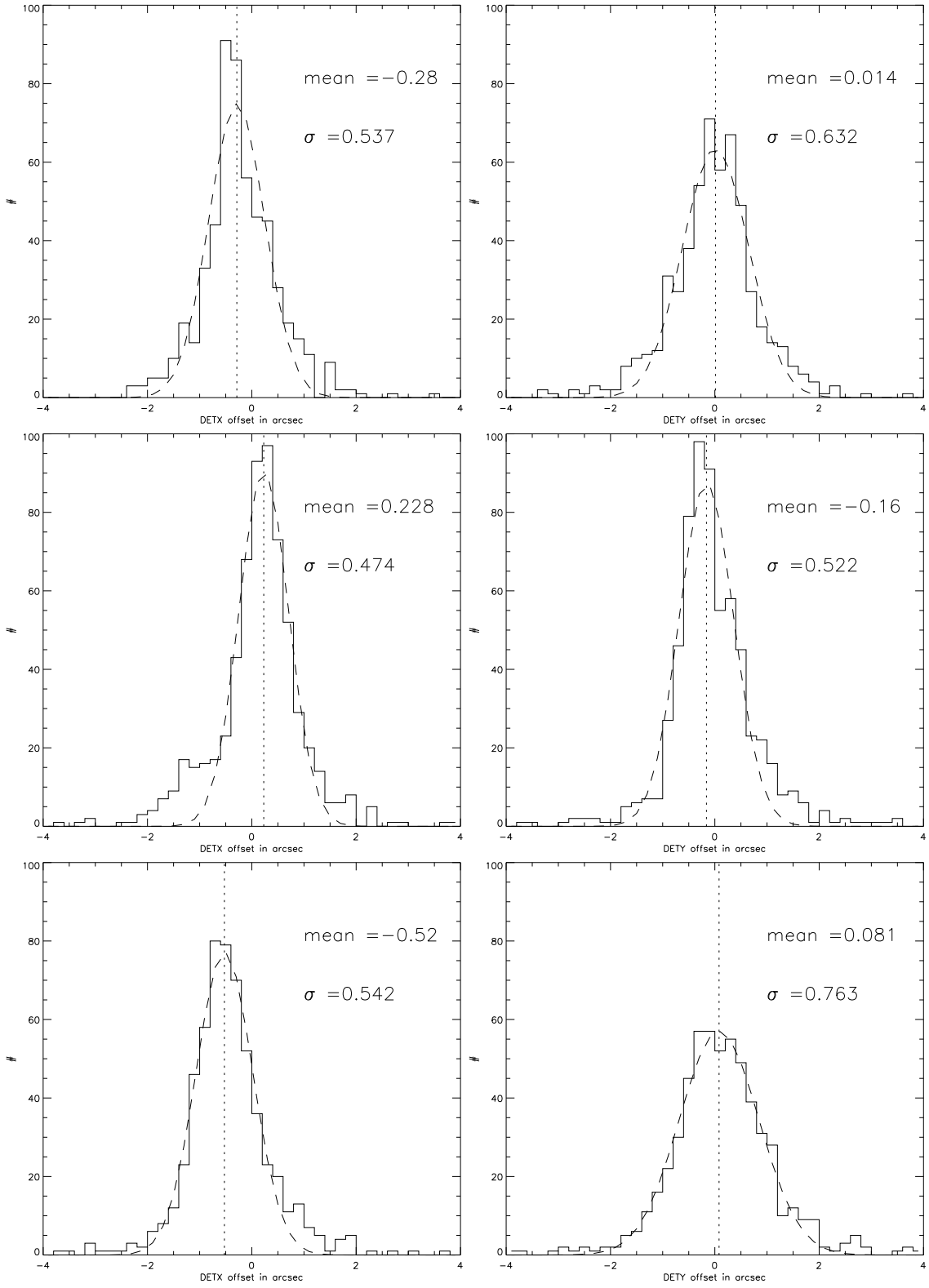

Figure 10: Histograms of the distribution of the offsets between EPIC cameras (in spacecraft axis) for all EPIC sources with more than 500 counts in the MOS central area (CCD1); Top panel: MOS1 vs EPIC-pn, Middle: MOS1 vs MOS2, Bottom: MOS2 vs EPIC-pn.

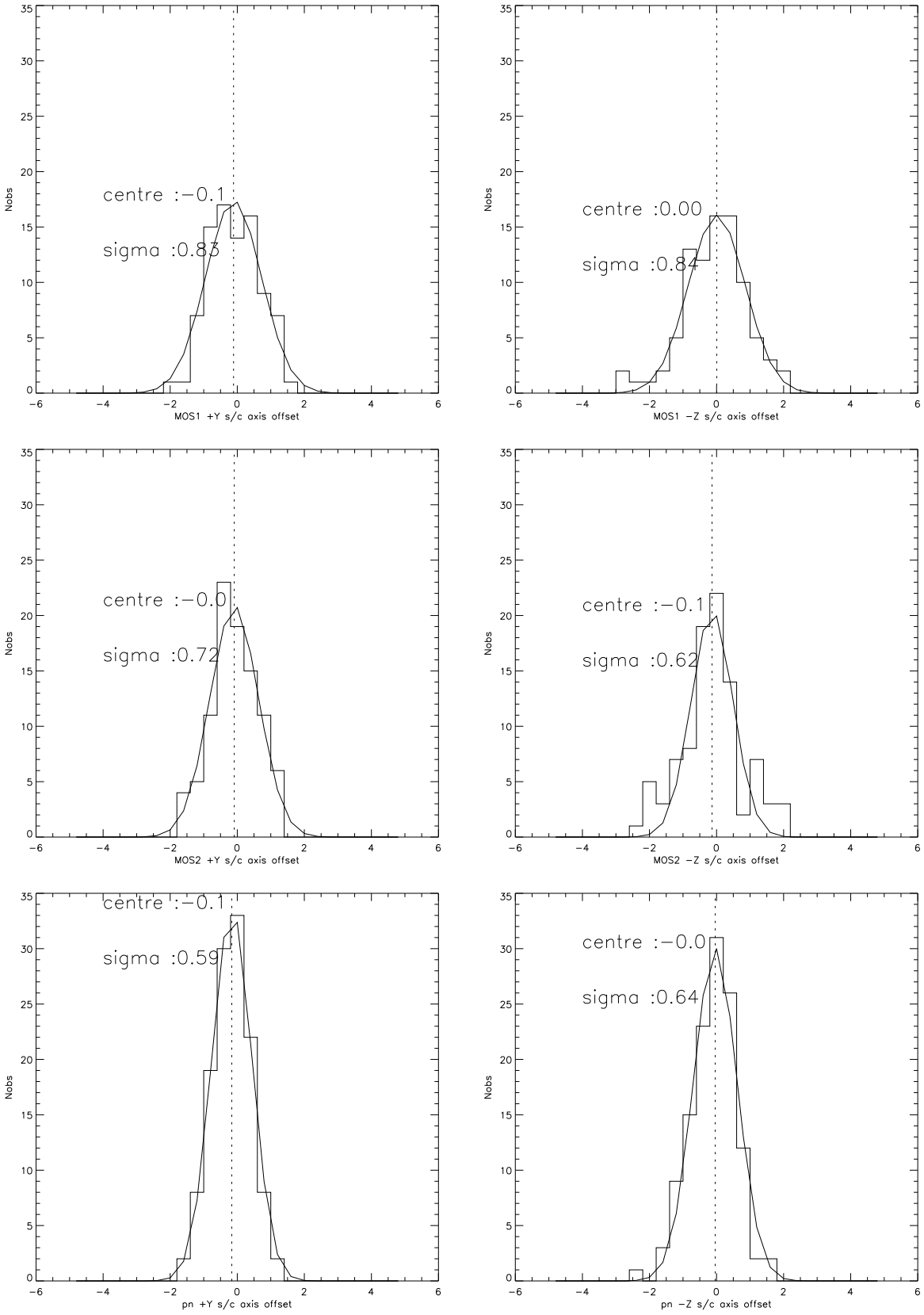

Figure 11: Histogram of the distribution of the offsets with the 2MASS reference frame for each EPIC on the two spacecraft axis with **BORESIGHT CCF v18** for a subset of exposures with more than 10 X-ray sources with 2MASS counterpart (on average 20-25). Top panel: MOS1, Middle: MOS2, Bottom: EPIC-pn.

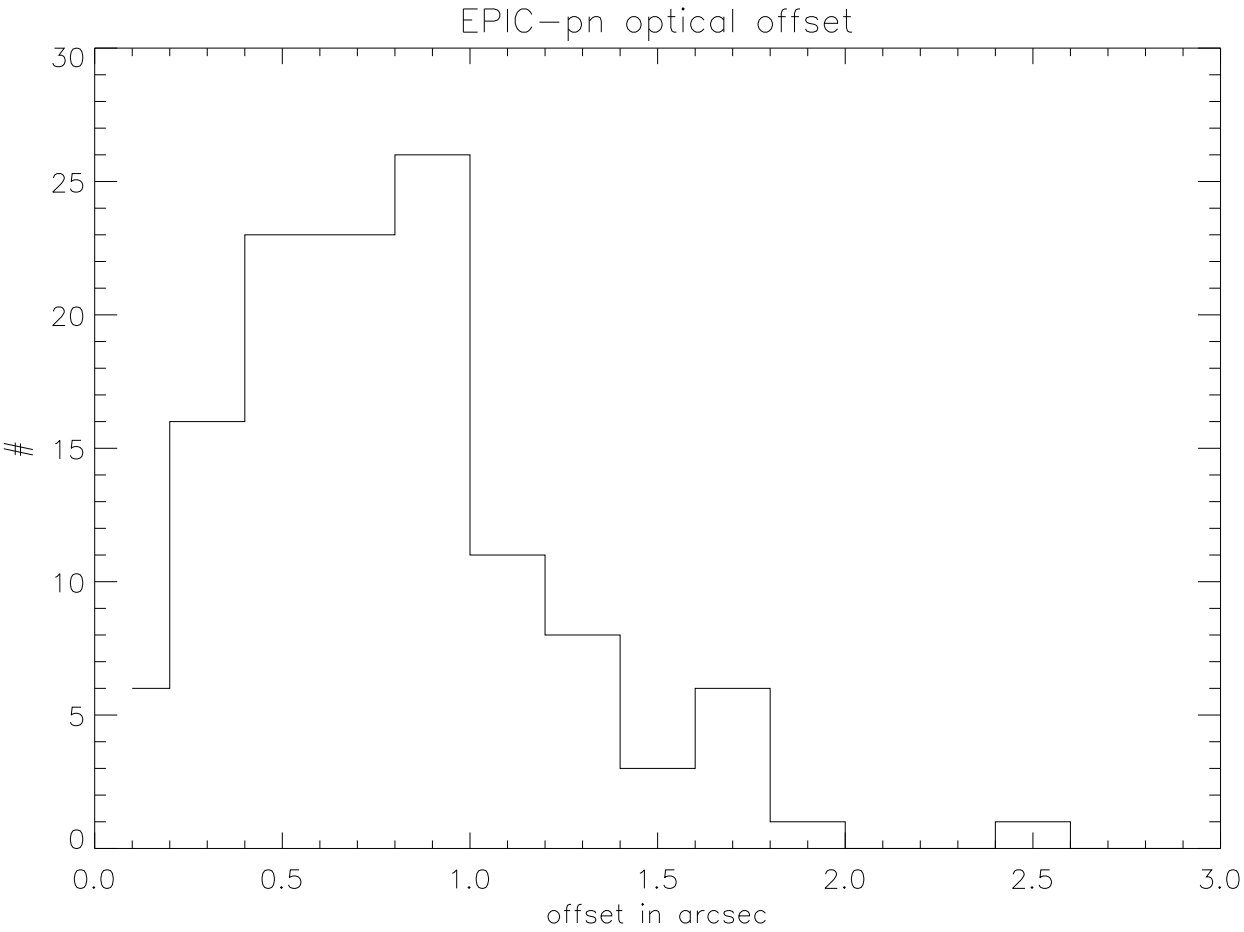

Figure 12: Histogram of the distribution of the offsets from the EPIC-pn frame to the 2MASS reference frame with **BORESIGHT CCF v18** for the subset of exposures with more than 10 X-ray sources with 2MASS counterpart (and on average 25)